Enhanced Geothermal Systems - Imaging and Characterization

Course Number: SU-02-111

PDH: 3

Approved for: AK, AL, AR, GA, IA, IL, IN, KS, KY, LA, MD, ME, MI, MN, MO, MS, MT, NC, ND, NE, NH, NJ, NM, NV, OH, OK, OR, PA, SC, SD, TN, TX, UT, VA, VT, WI, WV, and WY

New Jersey Professional Competency Approval #24GP00025600
North Carolina Approved Sponsor #S-0695
Maryland Approved Provider of Continuing Professional Competency
Indiana Continuing Education Provider #CE21800088

This document is the course text. You may review this material at your leisure before or after you purchase the course. In order to obtain credit for this course, complete the following steps:

1) Log in to My Account and purchase the course. If you don't have an account, go to New User to create an account.

2) After the course has been purchased, review the technical material and then complete the quiz at your convenience.

3) A Certificate of Completion is available once you pass the exam (70% or greater). If a passing grade is not obtained, you may take the quiz as many times as necessary until a passing grade is obtained (up to one year from the purchase date).

If you have any questions or technical difficulties, please call (508) 298-4787 or email us at admin@PDH-Pro.com.

Enhanced Geothermal Systems

Contact: Dan McMorrow — dmcmorrow@mitre.org

December 2013

JSR-13-320

Approved for public release; distribution unlimited.

JASON
The MITRE Corporation
7515 Colshire Drive
McLean, Virginia 22102-7508
(703) 983-6997

4 IMAGING AND CHARACTERIZATION

DOE has broad interests in characterizing the subsurface, and is therefore engaged with a variety of technologies for imaging and monitoring regions within Earth's crust (e.g., Snieder, et al., 2007) [25]. The needs of EGS are sufficiently distinct, however, that it is worth identifying promising opportunities for characterizing 1) regions being considered for future stimulation and production; 2) the spatial extent and characteristics of a stimulated volume; and 3) the spatial-temporal evolution of the region from which heat is being extracted.

Stimulation by hydrofracturing, for example, is expected to create vertical fractures because the principal normal stress is vertical at the depths being contemplated for EGS. Therefore, reflection seismology that is so heavily used in oil and gas exploration (because it typically gives the highest resolution over the greatest distances) needs to be performed at depth, in order to have near-normal incidence relative to the vertical fractures. This is in contrast to the (roughly) horizontal layering of oil and gas fields that allows data collection from Earth's (horizontal) surface for hydrocarbon exploration.

There is a tradeoff between range and resolution of features that can be imaged in the subsurface, with Figure 4-1 showing typical values for high-frequency seismic (kHz-MHz) and electromagnetic (MHz-GHz) methods. In detail, the values depend on material properties such as seismic-wave velocities and dielectric constant, the latter being especially sensitivity to the presence of moisture (a key factor in use of ground-penetrating radar, GPR). Nevertheless, resolution of meters or less generally requires imaging at distances less than tens to hundreds of meters, which implies getting sources and sensors near the region of interest.

This requirement of close-in imaging may be relaxed by turning to non-linear methods, which will be described in a subsequent section. We first describe an interferometric approach that can facilitate elastic imaging at depth.

4.1 Ambient-Field Seismic Imaging

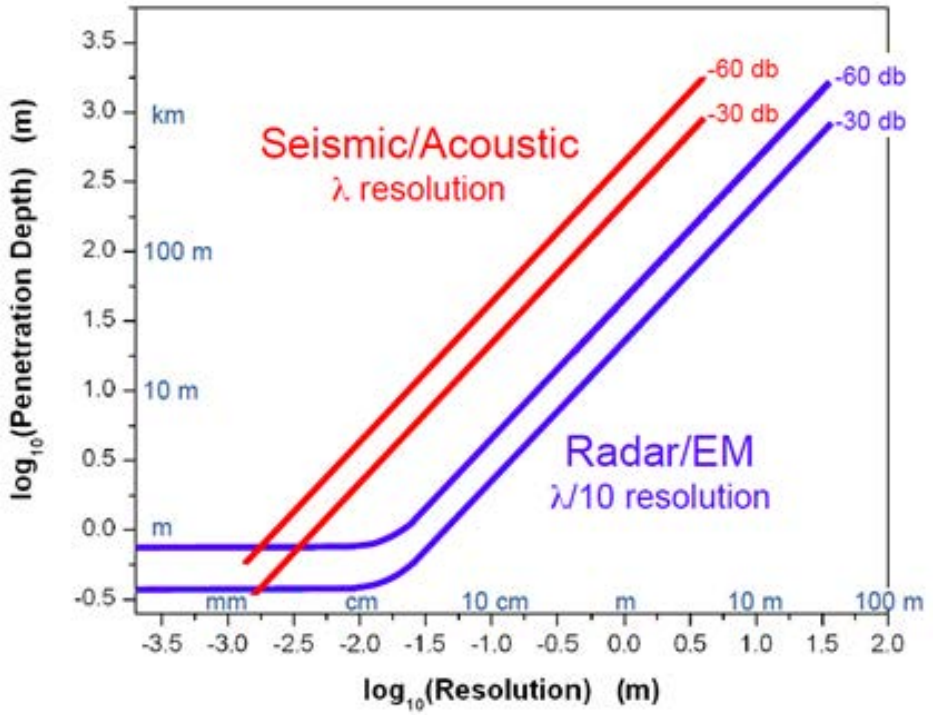

Figure 4-1: Calculated distances (penetration depth or range) over which high-frequency seismic (acoustic) and electromagnetic (Radar/EM) wave-based imaging can achieve a given resolution for return signals 3-6 orders of magnitude smaller than transmitted (-30 and -60 db). We assume linear elasticity and absorption (compressional-wave velocity and quality factor v_p = 5 km/s and Q = 100 at seismic frequencies of 100-1500 kHz; attenuation increasing from 2 to 20 m^{-1} at 15-1400 MHz and corresponding variations in dielectric constant for EM), with assumed resolution criteria (λ and $\lambda/10$, with λ being wavelength) that depend on processing methods used. The plot, applicable to high-resolution seismic reflection and ground-penetrating radar (GPR) measurements, implies resolution of 1 m at distances of order 10^2 and 10^1 m, respectively.

The only means of achieving near-normal incidence for vertical fractures at depth is to emplace sources and sensors in the subsurface. This is possible through conventional drilling, and may in the future be significantly enhanced by micro-drilling approaches we describe below.

A major development in seismology is to dispense with sources – which in this case would also need to be deployed at depth (and in different locations from the sensors) – through the use of interferometry. In particular, the ambient seismic field (background seismic noise) present in the crust can be used as a form of seismic "daylight" that illuminates the subsurface (Snieder and Wapenaar, 2010; Snieder and Larose, 2010) [26, 27].

The basic idea is to cross-correlate the signals from distinct detectors, effectively turning one sensor into a virtual source with respect to the other detector(s). With an array, which could simply be a string of detectors down a borehole, one has enough detector-pair combinations to be able to reconstruct images akin to those of reflection seismology, and so make possible imaging of vertical structures in the subsurface.

Ambient-field reflection seismology has been demonstrated from the surface (Figure 4-2) (Draganov, et al., 2007, 2009) [28, 29], with an application to imaging a geothermal field summarized by Tibuleac and Eneva (2011) [30], for example. In principle, one ought to be able to similarly image vertical structures in the subsurface through ambient-field seismic-reflection imaging in boreholes. In fact, the concept has been demonstrated through imaging of the San Andreas Fault from the side, in this case with nearby drilling serving as the source of seismic energy (Figure 4-3).

Snieder and Wapenaar (2010) [26] point out that shear-wave polarization can be used to determine fracture orientations at depth, and that cross-correlation of ambient seismic and electromagnetic fields can additionally provide a basis for characterizing subsurface permeability and fluid flow through poro-elastic effects. deRidder and Biondi (2013) [32] offer a recent

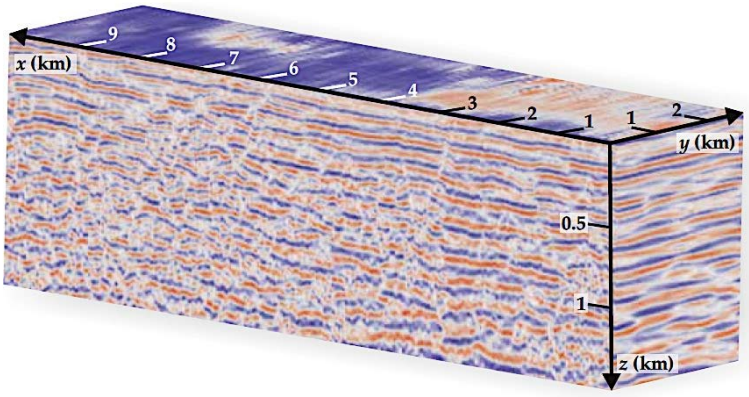

Figure 4-2: Three dimensional reflection image of crustal structure beneath the Libyan desert based on data obtained by cross-correlating 11 hours of ambient noise measured at the surface, illuminating horizontal discontinuities in seismic velocities (rock layers) at depth (Snieder and Wapenaar, 2010, based on results of Draganov, et al., 2009) [26, 29].

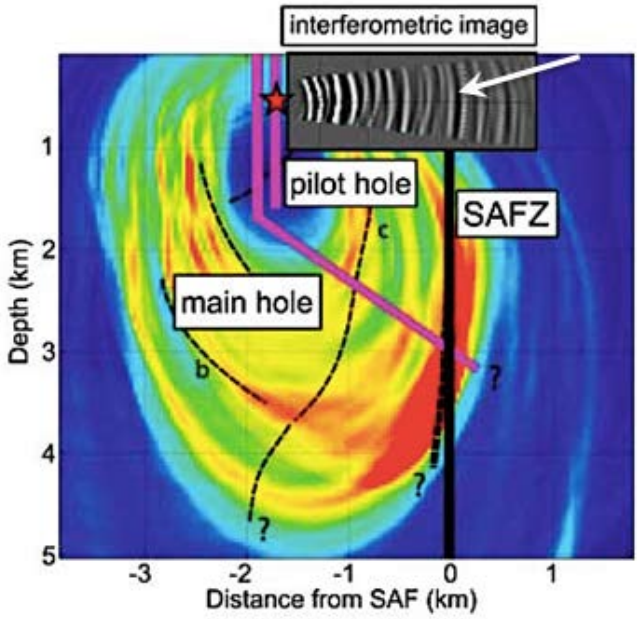

Figure 4-3: Interferometric image of the San Andreas Fault Zone (SAFZ) (*inset*) near Parkfield, CA, produced by recording in the pilot hole (*right magenta line*) drilling noise from the main hole (*left magenta line*), shows multiple reflections, including one due to the main SAF fault (*white arrow*). The target receiver used for imaging is indicated (*red star*), and the background color image (with thin dashed lines, question marks, and "b" and "c" labels) is from independent seismic imaging (colors indicate seismic-velocity variations) [31].

example of monitoring daily changes in an oil field at several hundred meters depth through ambient seismic noise.

4.2 Nonlinear Elastic Response

Nonlinear elasticity potentially offers unique benefits for subsurface imaging relevant to EGS. First, the nonlinear response of rock – deviations of observed strain from being directly proportional to the stress applied to a volume of rock – is highly sensitive to the presence of fractures under low effective stress (i.e., when fluid pressure inside the fractures closely matches the normal stresses due to overburden). The condition of low effective stress is of interest for i) identifying subsurface regions susceptible to stimulation for EGS; ii) quantifying the degree (success) and spatial extent of stimulation; and iii) monitoring the temporal evolution of a stimulated zone at depth.

Second, it is not individual fractures but the zone that is (incipiently) fractured that is imaged: that is, dimensions of meters to perhaps hundreds of meters instead of crack widths of millimeters to meters. Therefore, the need for spatial resolution is far less demanding than required for the usual linear-elastic imaging of structures (Figure 4-1).

The basic idea is that fractures can be opened and closed by externally imposed stresses, assuming a condition of low effective stress. The elastic response of a fractured volume differs greatly (non-linearly), depending on whether the cracks are in the process of opening up or are clamped shut (e.g., shear waves with polarization in the plane of the cracks being scattered or not, respectively). Therefore, regions of a rock insonified with a mix of, say, low-frequency waves (that open and close fractures, where present) and high-frequency pulses (that scatter off opening cracks) can in principle be used to reveal the presence of fractured zones (Figure 4-4).

Imaging depends on matching the timing, at each location in the rock volume, between high-frequency (probe) waves being present at a fracture

when the low-frequency (forcing) wave has the appropriate phase to open the crack rather than clamping it shut. In practice, the presence of cracks produces scattered waves at the sum and/or difference frequencies of the forcing and pulse frequencies, and localization is obtained by means of travel-time measurements to a detector array.

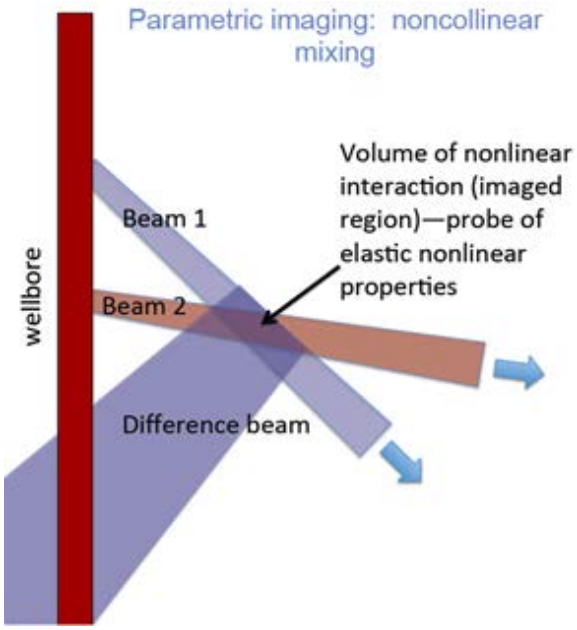

Figure 4-4: Schematic of nonlinear elastic imaging as applied to the subsurface, using arrays of transducers in a borehole to send two beams (low-frequency forcing beam plus high-frequency probe beam) in order to insonify and image a region of interest, as revealed by the difference (and/or sum) beam that emerges from the volume of nonlinear interaction (courtesy of P. A. Johnson).

Nonlinear elasticity of rock has been studied in the laboratory for more than 25 years, and shown to provide highly sensitive information about the presence, nature and spatial distribution of fractures, grain boundaries and other structural defects (e.g., Johnson, et al., 1987 [33]; Johnson and Shankland, 1989 [34]; Guyer and Johnson, 1999 [35]; Pasqualini, et al., 2007 [36]). One implementation that might be applied to the subsurface is documented by Kazakov, et al. (2002) [37], who showed that a crack insonified by a low-frequency wave is effective in scattering a high-frequency probe beam so as to produce an image of the crack (Figure 4-5); not surprisingly, the

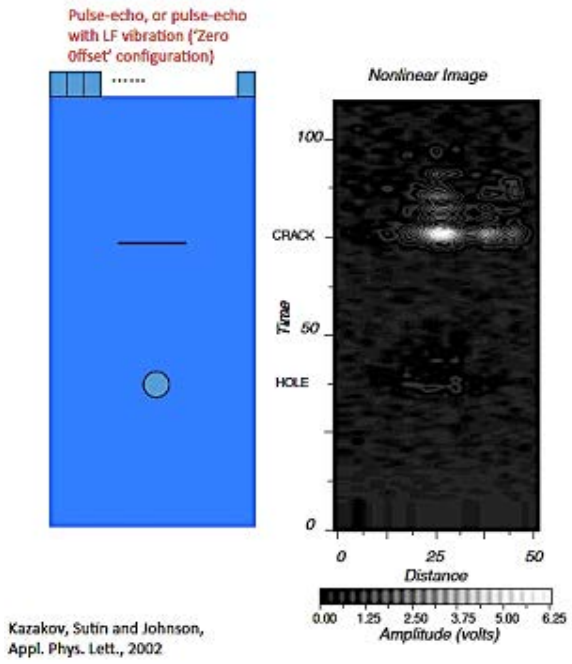

Figure 4-5: Laboratory demonstration of nonlinear elastic imaging of a crack in a steel plate that also contains a hole (after Kazakov, et al., 2002 [37]). The nonlinear image (*right*) shows the presence of the crack, as illustrated in the schematic (*left*). Because of its thin dimension, the crack is barely visible in a linear-elastic image (not shown).

crack was nearly impossible to resolve by standard (linear-elastic) methods. If scaled up from laboratory to field distances, nonlinear elasticity could offer an important advance in subsurface imaging relevant to EGS.

Time-reversal imaging of nonlinear elastic response is established as a means of non-destructive evaluation of materials at the laboratory scale (e.g., Ulrich, et al., 2008) [38]. What now needs to be done for application to EGS is to validate this method at field scales of tens to hundreds of meters in order to determine the practical ranges and sensitivities of the method. For example, over what distances can cracks be sufficiently insonified to produce a nonlinear elastic response, and is background (elastic) heterogeneity of the rock small enough to allow nonlinear imaging at ranges of interest? Initial field experiments do not need to be performed at great depth (e.g, meters to tens of meters would be sufficient, rather than the km depths of EGS),

and would mainly be used to document tradeoffs between range, resolution and sensitivity that can be achieved. The potentially confounding effects of background clutter are unlikely to be important at distances of meters (i.e., not much larger ranges than achieved in the laboratory), so there is much information to be gained as one scales up to distances of tens and then hundreds of meters. Subsequent work could take the field experiments to greater depths.

In addition to characterizing the quality of signal that can be acquired, there will be practical considerations of equipment and configurations to be used. For example, low-frequency insonification might best be driven from the surface, using Vibroseis or related technologies, rather than via down-hole transducers (Figure 4-4). Optimal frequency ranges will also have to be determined.

In this regard, seismic energy is not the only means of applying a forcing stress (or strain) to a volume of subsurface rock. Changes in temperature cause thermal strains, and these have again been shown to produce nonlinear changes in elastic properties that can be used to image damage zones – at least at laboratory scales (e.g., Ohara, et al., 2013) [39]. Another form of low-frequency forcing comes from natural tides that stress Earth's crust with a well-known spectrum of periodicities and may therefore be able to reveal modified properties of freshly stimulated regions at depth. It is further conceivable that seismic daylight, as described above (ambient seismic field), could be used to image the resulting nonlinear elastic response.

In summary, there are opportunities for developing nonlinear elastic imaging to document thermal and other time-dependent changes of rock that are relevant to EGS characterization at depth in the crust.

4.3 Drilling

Drilling plays many roles for EGS, from exploration and characterization of likely sites to development and production of a field [40]. Because drilling is so important to characterization of the subsurface, whether by directly sampling the rock at depth or by providing access for other instrumentation (e.g., seismic and electromagnetic sensors described above, as well as tracer experiments discussed below), we discuss drilling technologies next. However, this text applies just as well to EGS creation and production, as discussed in a later section. We recognize that explosives can be used to complement drilling for EGS, and encourage consideration of this technology, as well.

Many of the challenges that arise with drilling for EGS are the same as arise in drilling for hydrocarbons (see Maurer, 1980) [41]. EGS thus can take advantage of technologies developed for the much larger hydrocarbon industry.

4.3.1 Conventional holes

Drilling is based on applying shear stress by friction with a hard bit pressed against rock, leading to tensile and shear failure behind and around the sliding contact. This is particularly important for hard rock because the shear strength is significantly less than the uniaxial compressive strength (e.g., 200 MPa versus 5 MPa for granites). Drilling for conventional geothermal has been among the most challenging drilling activities because the rock is hard and the holes must be large. Polycrystalline diamond compact (PDC) bits now widely used in other applications (oil and gas) were originally developed 30 years ago for geothermal drilling. There have been modest improvements in the relevant conventional drilling technology with PDC, and they are becoming more widely used than conventional roller cone bits. Schlumberger reports a 1/3 increase in average run lengths for its newest bits for high-temperature hard rock drilling (Schlumberger, 2012) [42].

Some new materials have been developed. Further improvements in PDC have been reported by SNL, drilling a 3000 ft geothermal well at an average rate of 30 ft/hr over four days, three times better than standard roller cone bits (Sandia, 2012) [43]. These compacts have been improved by the use of microwave sintering (e.g., tungsten carbide to diamond composites). Other materials potentially useful for hard rock include nanopolycrystalline diamond (Nakamoto et al., 2011) [44] and tough CVD diamond (Liang et al., 2009) [45], which have been proposed for deep drilling. Though tougher than polycrystalline diamond, wear resistance tests in the field have not been done.

4.3.2 "Microholes"

Developing technology for rapid drilling of small holes is of interest to both the hydrocarbon industry and EGS for exploration and seismic sensing (noise levels are much lower even at a few hundred feet of depth than at the surface, and EGS requires monitoring microseisms that indicate fracturing). Conventional deep big holes start at >20" diameter and taper down with progressively smaller casing reaching 6-7" at depth. Microholes are defined as those less than 5", typically 2-2.5" which would give a 1" ID hole with casing. In comparison to the larger holes, the casing can be light, there is significantly less hole waste and rock damage, and they can be drilled quickly to minimize cost and to allow more extensive and accurate monitoring. Real and perceived potential hazards from induced seismicity, as well as its use as a mapping tool provides additional impetus for developing better monitoring of EGS systems. Tomographic monitoring is accomplished from a distribution of holes containing an array of geophones. Another driver for small holes has been gas control for coal mine safety (Lu et al., 2013) [46].

As described by Majer (2013) [47], the target is for boreholes that (a) can be drilled at 100 to 200 ft/hr to minimize cost, (b) extend to depths of at least 5000 ft at these high drilling rates; (c) have minimum waste, which maximizes speed while minimizing permitting issues; (d) have small

rig footprint, for rapid deployment as well as minimizing permitting issues; (e) have minimum formation damage to borehole walls and surrounding rock to improve monitoring; (f) have a small diameter that allows better seismic coupling of instrumentation to the rock.

For many technologies, drilling in homogeneous hard rock is straightforward. Encountering zones in which pressure is lost by washout, fractures, faults, and boundaries between rock types creates difficulties. Then balance must be struck between drilling pressure (air, water or mud) and the formation pressures/fluids (rock and fluid). Small holes would require an order of magnitude less material than conventional holes, a significant saving.

A program to develop both the drilling and the sensor technology was started by the DOE in 2005 but ended within a couple of years (Long, 2005; 2007) [48, 49]. It led to developments that included technologies for drilling small holes such as resonant drilling, high pressure fluid enhanced cutting, and high-speed drilling. Laser drilling and microwave drilling were also considered but remained far from proven in the field. The program also showed that small holes can accommodate small geophones and other tools (Long, 2007) [49], such as 3 mm Fabry-Perot MEMS accelerometers for seismic imaging (Lumedyne). Mapping with accelerometers/tilt meters was begun (Pinnacle Technologies), with tests carried out at the NSF-funded San Andreas Fault Observatory at Depth (SAFOD).

Reaching >5000 ft with microholes would provide the opportunity for arrays for 'horizontal' imaging as discussed in Sections 4.1-4.2. The lower noise and better coupling of instruments in shallower microholes may enable more extensive vertical seismic profiling up to four times the hole depth (Majer 2013) [47]. Vertical seismic arrays permit both active and passive seismic monitoring. Active monitoring examines fine scale structural features, including the locations of fractures/faults. Passive monitoring provides information on the dynamics of the fracture creation and induced seismicity resulting from changing stress.

Equipment that may be used in microdrilling is shown in Figure 4-6. The equipment for coiled tubing drilling (CTD), a method of drilling narrow diameter holes in which a drill bit driven by a motor in a bottom hole assembly (BHA), is contained within a lining of flexible narrow-diameter tubing that is unrolled from a coil. Unlike conventional drilling, there is no rotating drill string extending from the surface and no need to withdraw and relower it many times to add additional pipe. CTD is not a new technology, but has chiefly been used in well completion and re-entry, rather than as the principal means of drilling a new hole. However, it may become the optimal means of drilling narrow holes for emplacing sensors at depth or *in situ* measurement of rock properties.

Figure 4-6: Coil tubing rig capable of 1500 foot hole developed by LANL.

4.3.3 Resonant drilling

In rotary drilling, fluid is required to move the drilled material out of the way of the bit. Flushing media for sonic drilling can be as simple as

air and water. A sonic drill bit oscillates vertically, thus creating turbulent flow at the drilling interface that pushes loose drilled material aside. When flushing media are required, the actual amount required is small compared to rotary drilling.

Sonic (termed resonant, because a drill pipe is oscillated at its lowest resonant frequency) drilling is being developed for comparatively shallow wells, generally in soft or unconsolidated material. It may be useful for drilling the shallow wells (to 500 ft) needed in larger numbers for emplacement of seismic sensors. Drilling rates have been reported to be several times faster than for conventional drilling. Whether or not it can be applicable to deeper drilling for EGS injection and production wells will require additional research and development. Critical factors include the need to balance the force of a long drill string to promote cutting without fusing of the tip with the rock, damping losses due to contact with the borehole walls, and changes in rock properties with depth (see Lucon, 2013) [50].

4.3.4 Fluid injection drilling

Abrasive jet cutting was proposed early on for drilling (see Kolle, 1999) [51]. H_2O or CO_2 can be used as the fluid. Use of a CO_2 slurry mix, nozzle and high-pressure slurry pump has been demonstrated in the lab to have high penetration rates in basalt. If a larger bore is required, rotation of the nozzle(s) can be provided with a small down hole hydraulic or electric motor. The pump accelerates and pressurizes the slurry. A nozzle can be focused to concentrate the slurry stream on the periphery of the drill hole, reducing the work required, as demonstrated in the 1960s (Maurer, 1980) [41]. Limited field studies have been conducted with small coiled tubing (for example with 1" OD tubing). The entire bottom hole assembly is inexpensive such that the coiled tubing can be cut and cemented in place when the desired depth is reached.

The original CO_2 technique grew out of the technology developed by LANL, and has been used for drilling to 1500 ft. High pressure (3000 – 5000 psi) is used to cut through the rock. There is near zero "weight on bottom hole", gravity guiding the drilling direction. LANL used this to drill 1.25" ID holes in which 48 levels of geophones (0.85" OD sensors) were mounted. A surface pumping system mixes the proper fluids and solids concentration and pressurizes such slurries. High pressure pump systems developed for these slurries operate at up to 15,000 psi and 15 gal/min.

Abrasive jet drilling has not succeeded in drilling deep holes because of the difficulty of handling and delivering the amounts of abrasives required at depth, the need to balance the high-pressure of the jet with the pressure of fluid in the hole, and difficulties in steering. Wear on the nozzles by the abrasive could be reduced with the use of toughened materials discussed above (e.g., diamond-based materials). Work continues on developing hybrid technologies that involve abrasive jets and impact drilling (e.g., Lu et al., 2013 [46]) but field tests in EGS-relevant environments apparently have not been reported.

4.3.5 High-speed dual string drilling

High-speed ($\sim$ 5000 rpm) grinding mechanisms (Figure 4-7) must put very little weight on the bit because the frictional power dissipated is proportional to the product of the rotation rate, the applied force and a coefficient of friction (Kolle, 1996) [52]. This method produces pulverized stone with sub-millimeter particles, in contrast to the large broken up rock typically produced from slow grinding (Able, 2013) [53]. The lower weight on the bit produces less wear. Both diamond impregnated bits and PDC have been used. The first high-speed dual string system will be tested in the field this year.

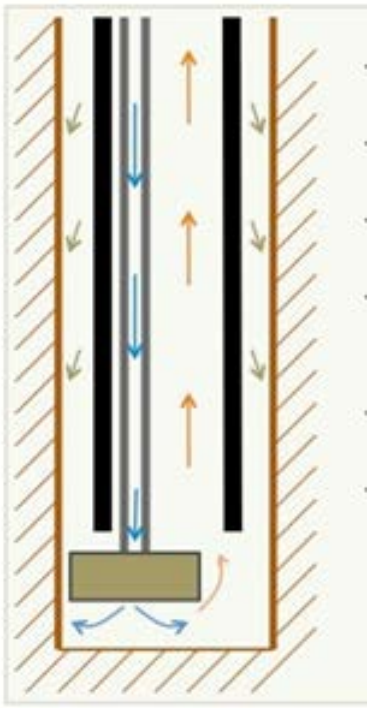

Figure 4-7: Schematic of a high-speed dual string drilling (Able, 2013) [53].

4.3.6 Summary

In summary, although we are not aware of any single breakthrough technology, developments that may lead to drilling small holes for exploration and monitoring warrant further study. These may take advantage of continued developments of small deployable sensors for downhole monitoring, including imaging. Overall, we conclude that microhole research and development begun during the past decade should be followed up with the appropriate field tests.

4.4 Physical Description and Time Evolution of an EGS Reservoir

It is useful to describe in order of magnitude terms the basic physical processes associated with fluid flow, heat transfer and tracer transport as all

are important for the response and characterization of the thermal system. First, we assume that hydraulic or other fracturing operations occur, which produce a crack-like network, that is combined with existing fractures and faults in the rock (Figure 4-8). Ideally, the fracture network extends from the injection well to the production well, but the spatial characteristics (e.g. typical dimensions and the heterogeneity) of the fracture network are a significant unknown. A major goal of subsurface imaging and characterization is to more accurately determine the spatial structure of the flow network. Because Earth is effectively an elastic medium, albeit with nonlinear and time-dependent, hysteretic (viscous) properties, the flow network, e.g. the typical crack openings, can evolve in response to time varying applied pressures.

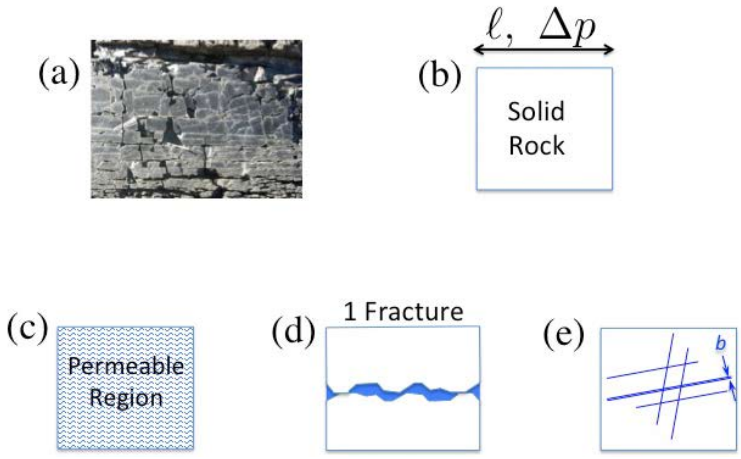

Figure 4-8: Models of a fracture network in a rock. (a) Image of a typical rock in the field setting (S. Petty briefing to JASON). (b) A pressure drop Δp is applied between injection and production wells a distance ℓ apart in order to extract energy from hot rock in the subsurface. (c) The subsurface may be modeled as uniformly permeable. (d) A single fracture produces a local region of high permeability in a region of otherwise low permeability. (e) A network of cracks: as discussed in the text, the flow rate is proportional to b^3 ("cube law"), so is dominated by the widest crack.

For now we simply assume that a fracture network exists. It is natural to expect that the network has a distribution of channel openings (b), which represent the smallest dimensions in the network, spans a distance $h \gg b$

perpendicular to the flow and is in the plane of the crack (for a simple uniform crack), and lengths $\mathcal{O}(\ell)$, where ℓ is the distance between the injection and production wells. We assume $b \ll h \lesssim \ell$ (see Figure 4-9).

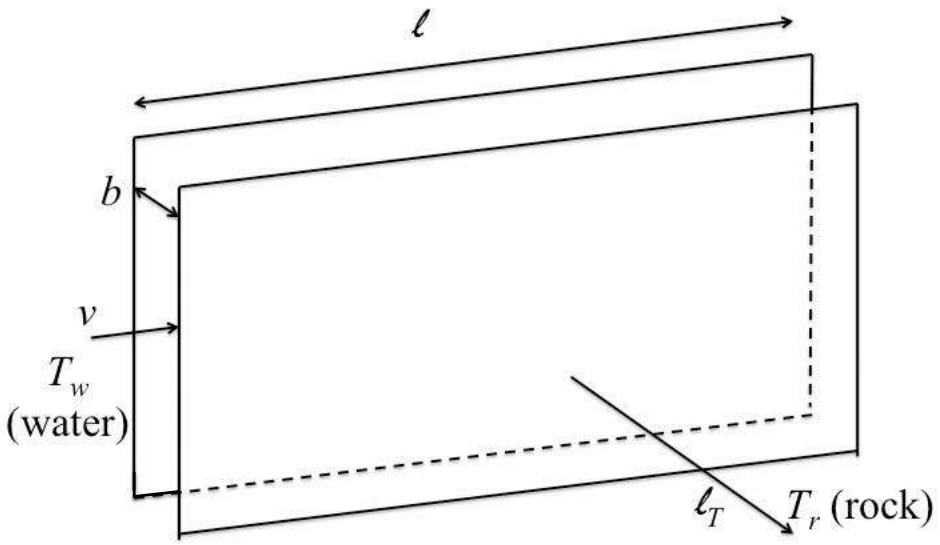

Figure 4-9: Schematic of the model geometry for flow in a crack of width b, with other common notation indicated.

4.4.1 Some characteristic scales of the crack network for flow and heat transfer

If a crack opening b is too large then fluid flows rapidly through it without being heated close to the rock temperature. Even if energy is extracted, the Carnot efficiency of water in an energy producing cycle is low. Also, if crack openings are too narrow, their low hydrodynamic admittance (or large viscous resistance) requires more hydrodynamic work and a higher pressure drop between injection and production wells in order to extract the desired power. Note that generation of geothermal energy is implicit in our assumption of a characteristic time scale of energy extraction, which, practically, is

determined by economic considerations of return on investment; we do not attempt any economic analyses here.

We first determine a characteristic width[1] b_0 of a crack in EGS, defined as the typical width of the cracks that draw heat approximately uniformly from the entire volume penetrated by cracks. We note that the actual crack widths in the reservoir need not be equal, or even comparable, to b_0 (though we later show they must not exceed b_0 for efficient generation of geothermal power); b_0 only defines a physical scale characterizing the coupled fluid flow and heat transfer. This characteristic width is a function of the parameters of the resource. We consider cracks of width b, length (between injection and production wells) ℓ, and transverse (spanwise) dimension h (that does not enter); typically we take $h = \ell$.

When making estimates below we will use the thermal diffusion coefficient $\kappa_r = 10^{-6}$ m^2/s ≈ 30 m^2/yr for rock, volumetric specific heats of rock $C_r = 2.5 \times 10^6$ J/m^{3}K and of water $C_w = 4.2 \times 10^6$ J/m^{3}K, pressure drop $\Delta p = 100$ bar, viscosity of water at a mean temperature of 100 °C is $\eta = 3 \times 10^{-4}$ kg/m-s, and a crack length $\ell = 10^3$ m. Also, we will typically assume a system age $t_r = 10$ years.

To heat the water efficiently in a crack of width b we equate the thermal energy (per unit area) carried by the water as it is heated by an amount ΔT_w over a length ℓ

$$\frac{\Delta T_w C_w v b}{\ell}, \tag{4-1}$$

where v is the mean flow speed, to the conductive heat flux out of the rock,

$$\frac{2 k_r \Delta T_r}{\ell_T}, \tag{4-2}$$

where k_r is the thermal conductivity of rock, ΔT_r is the temperature drop between the deep hot rock and the water and thermal conduction sets the minimum length scale, $\ell_T = \sqrt{\kappa_r t_r} \approx 18$ m, of temperature gradients in the rock assuming a 10 year time scale. The factor of 2 accounts for the two

[1]By "width" of a crack we mean the distance separating its two, nearly planar, surfaces, which is generally quite small compared to other length scales in the system.

surfaces of a planar crack. Cracks spaced closer than $\mathcal{O}(2\ell_T)$ effectively draw on the same thermal resource, although their hydrodynamic admittances add, reducing the pressure drop and mechanical work required to extract the same amount of heat.

For efficient operation of such a geothermal system we desire $\Delta T_r \ll \Delta T_w$, which is equivalent to requiring that the water be heated to a temperature close to the rock temperature far from the cooling flow. For viscous flow in a duct, the mean speed is

$$v = \frac{\Delta p}{\ell}\frac{b^2}{12\eta}. \tag{4-3}$$

This law is generally written in terms of the two-dimensional flow rate $q = vb$, in which case $q \propto b^3\Delta p$, which is sometimes known as the b^3 law. The use of this simple channel flow formula for cracked materials relevant to the solid Earth has been verified (Witherspoon, 1980) [54]. One simple consequence of the b^3 law is that for any system characterized by cracks in parallel the flow predominantly goes through the widest paths of lowest fluid resistance, which is the simplest form of bypassing the hot rock. Not surprisingly, such channeling has been suggested as one reason for low heat recovery factors (e.g. [1, 22]).

Combining equations (4-1 to 4-3), we find

$$b < b_0 \equiv \left(\frac{C_r}{C_w}\sqrt{\frac{\kappa_r}{t_r}}\frac{24\ell^2\eta}{\Delta p}\right)^{1/3}. \tag{4-4}$$

Inserting the typical numbers above, $b_0 = 0.027$ cm and the corresponding $v_0 = 22$ cm/s. Water flowing in a wider crack has faster speeds for the same pressure drop and well spacing ℓ, is heated less and does not approach the distant rock temperature. Although it is capable of removing thermal energy effectively from the rock, the lower water temperature reduces the thermodynamic efficiency of electric power generation.

The characteristic Reynolds number for such a typical crack is

$$\mathrm{Re}_0 = \frac{3\rho v_0 b_0}{4\eta} = \frac{\rho b_0^3 \Delta p}{16\eta^2\ell} \approx 160, \tag{4-5}$$

where the factor of 3/4 comes from using the central (peak) velocity $3v_0/2$ and $b_0/2$ as the length scale, in analogy to the use of the radius to define the Reynolds number of a circular pipe flow. The flow in a crack thin enough for efficient heat transfer to the fluid is laminar, but if it is wide enough to be an efficient heat sink (turning the inequalities into approximate equalities) then it is likely that $\mathrm{Re} \gg 1$.

If parametrized in terms of volumetric flow rate Q, taking the span of the crack to be $h \approx \ell$, the same as its length, the crack width drops out. The result is a condition on the flow rate Q in a single "characteristic" crack:

$$Q < Q_0 \equiv \frac{2C_r}{C_w}\sqrt{\frac{\kappa_r}{t_r}}\ell^2 \approx 60 \left(\frac{\ell}{1\,\mathrm{km}}\right)^2 \mathrm{l/s}, \tag{4-6}$$

where again we have made numerical estimates based on the typical parameters above. This value of Q_0 is comparable to the flow rates of entire EGS systems. If cracks have widths $b \approx b_0$ only one or a few may be contributing significantly to the fluid flow. A total flow rate $\lesssim Q_0$ implies that the temperature of the (initially) produced hot water is close to T_r, as observed. Were there only one contributing crack, it would be predicted that increasing the flow rate above Q_0 would immediately reduce the temperature of the produced water. Were there many contributing cracks, the temperature would not immediately be reduced, and the condition (4-4) for efficient use of thermal energy need not be violated. One conclusion from this kind of interpretation is that the dependence of produced water temperature on forced flow rate is a possible test for the number of significantly contributing cracks.

We return to discuss more about the thermal characteristics for heat transfer in the reservoir in our discussion of EGS energy production in Section 5.

4.5 Tracer Experiments and Models

It is important to use all possible tools to characterize the reservoir. Two kinds of tracers have been investigated, chemical tracers and thermal

tracers. The traditional means for studying transport processes in porous media are breakthrough studies where a tracer is injected at one well and extracted at another well; such studies are well described in the literature (e.g. [55, 56, 57]). These experiments are typically several days to a week in length and give at best an average characterization of a heterogenous medium, so it is important to consider faster methods as well as methods with more spatial resolution for characterizing the reservoir. Alternatively, injection for some time followed by withdrawal from the same injection well, so-called injection/withdrawal tests, are described also, but less frequently (e.g. [58, 59]).

Two characteristics that can possibly be estimated by tracer experiments are a measure of the permeability of the reservoir and some features of the local heat transfer from the reservoir to the water (these are obviously linked). Possible advances to achieve higher spatial resolution of the permeability variation may be feasible with electromagnetic monitoring of electrically conducting fluids likely in combination with injection/withdrawal tests (see Section 4.6).

4.5.1 Breakthrough curves from tracer studies

It is useful to first analyze the traditional characterization study where a tracer is injected at one location (the injection well) and the time history of a concentration profile is then measured at the production well. There is a large classic literature on this topic, including detailed studies on the broad topic of transport in porous media (e.g., [60]), and here we summarize the simplest one-dimensional model, which may give some insight into transport in systems. For simplicity we consider a one-dimensional situation where the average concentration $c(x,t)$ evolves according to (think of this as the average concentration over the dominant flow paths from injection to production wells)

$$\frac{\partial c}{\partial t} + v\frac{\partial c}{\partial x} = \mathcal{D}\frac{\partial^2 c}{\partial x^2} \tag{4-7}$$

where v is the average speed in the channel (here v is assumed constant) and $\mathcal{D}$ is the longitudinal dispersion coefficient, which here is assumed constant. In the spirit of the single-channel analysis summarized in Section 4.4.1 we note that for the conditions typical of laminar flows in a single long narrow channel the dispersion coefficient is given by the Taylor-Aris result [61]:

$$\mathcal{D} = D_m + \frac{1}{210}\frac{v^2 b^2}{D_m} \quad \text{or} \quad \mathcal{D} = D_m\left(1 + \frac{1}{210}\mathcal{P}_b^2\right), \tag{4-8}$$

where D_m is the molecular diffusion coefficient and the Peclet number is $\mathcal{P}_b = \frac{vb}{D_m}$. When $\mathcal{P}_b \gg 10$, the longitudinal dispersion is dominated by the flow with $\mathcal{D} \propto v^2 b^2/D_m \gg D_m$. This one-dimensional interpretation based on a single uniform channel is obviously an idealization and does not rationalize field data we describe below. Instead, the dispersion coefficient $\mathcal{D}$ in equation (4-7) should be interpreted as an empirical parameter characterizing the flow in the crack network.

Consider the case where an injection of a tracer is localized in space at some time $t = 0$, i.e. a delta function release of a fixed amount, $A = \int_{-\infty}^{\infty} c(x,t)\ \mathrm{d}x$, with $c(x,0) = A\delta(x)$. Then the classical solution to the convective-diffusion equation is

$$c(x,t) = \frac{A}{\sqrt{4\pi\mathcal{D}t}} e^{-(x-vt)^2/(4\mathcal{D}t)}. \tag{4-9}$$

One way this result can be used is to record a measurement at the production well, a distance ℓ away. Then the recorded signal, or breakthrough curve, is a function of time given by

$$c(\ell,t) = \frac{A}{\sqrt{4\pi\mathcal{D}t}} e^{-(\ell-vt)^2/(4\mathcal{D}t)}. \tag{4-10}$$

It is convenient to rewrite this equation in dimensionless form as

$$\frac{c(\ell,t)}{A/\left(\ell\sqrt{4\pi}\right)} = \frac{\sqrt{\mathcal{P}_\ell}}{\sqrt{\tau}} e^{-\mathcal{P}_\ell(1-\tau)^2/(4\tau)} \equiv C(\tau), \tag{4-11}$$

where

$$\tau = \frac{tv}{\ell} \quad \text{and} \quad \mathcal{P}_\ell = \frac{v\ell}{\mathcal{D}}. \tag{4-12}$$

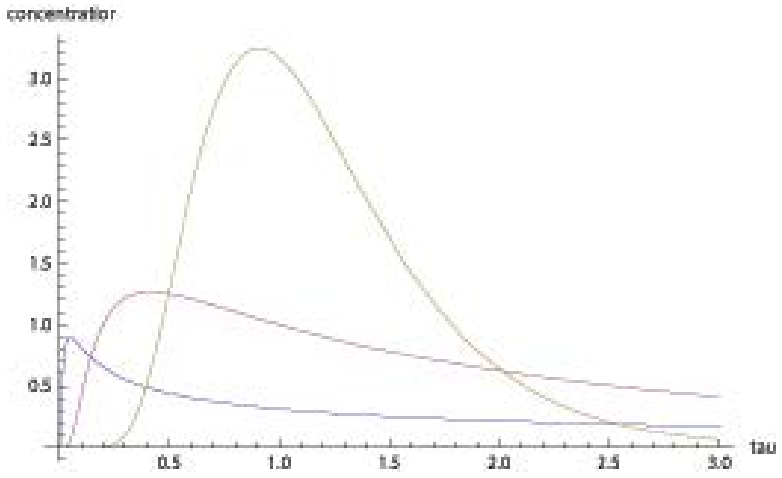

Figure 4-10: A plot of model breakthrough curves based on a one-dimensional convective-diffusion equation. Peclet numbers 0.1 (lowest magnitude), 1 (middle) and 10 (highest magnitude) are shown.

Typical theoretical breakthrough curves for different $\mathcal{P}_\ell$ are shown in Figure 4-10.

We have examined several breakthrough curves reported in the literature. For example, in Figure 4-11(a) we show the results of a typical field experiment from the Soda Lake geothermal site [62]; the red curve shows the results for a conserved, non-sorbing tracer. We note that the shape is qualitatively similar to the one-dimensional model. In addition, in Figure 4-11(b) we show data reported for breakthrough curves at the Steamboat geothermal reservoir and again the shape is qualitatively similar to the one-dimensional model. Next we investigate these results more quantitatively. Note that it is tempting to simply estimate the mean speed v by identifying the maximum in the breakthrough curve, which occurs at the time t_m, and then calculate the mean speed $v \approx \ell/t_m$. This estimate becomes increasingly inaccurate as the breakthrough curves show increasing degrees of longitudinal dispersion, as we quantify below. Next we take a closer look at this field data.

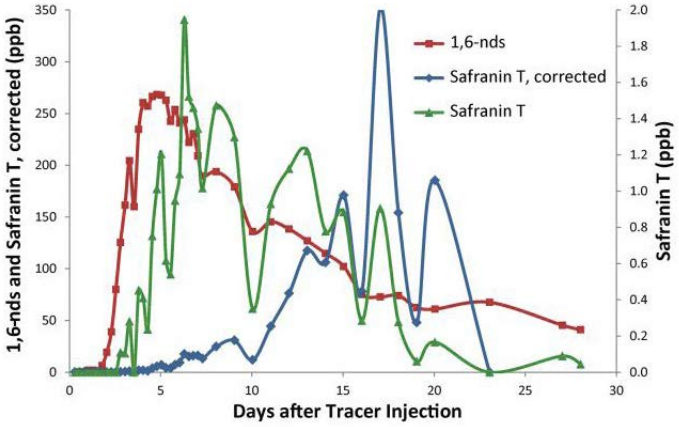

(a)

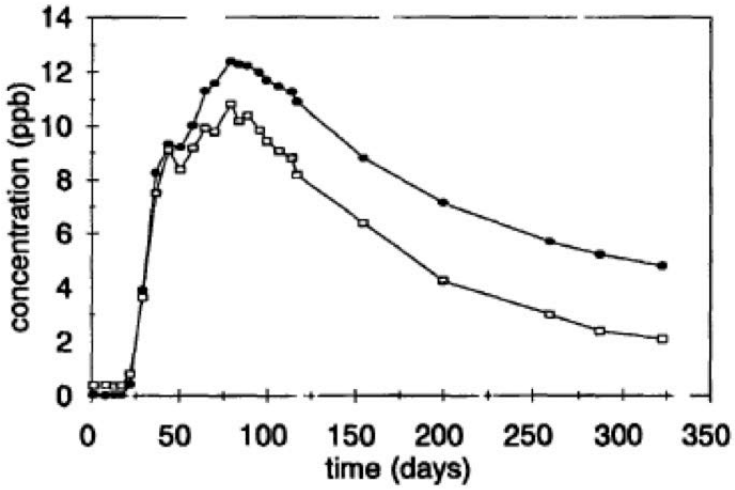

(b)

Figure 4-11: (a) Breakthough curves from field experiments at Soda Lake, Nevada [62]. The red curve is the response of a conserved, non-sorbing tracer, which is analyzed in the text. (b) Breakthrough curves from field experiments at the Steamboat geothermal site [63]. The upper curve is for a non-sorbing tracer, while the lower curve uses a chemical that degrades in time owing to thermal effects.

4.5.2 Order-of-magnitude estimates for the breakthrough curves

We can obtain some numerical estimates of the properties of an actual dry rock geothermal resource from a tracer experiment at Soda Lake [64, 62]. In this experiment the injection and production wells were 550 m apart and the pressure differential, provided by a 1360′ pressure head and an additional 110 psi on the injection well, was 48 bars, for a pressure gradient $\frac{\Delta p}{\ell} \approx 9 \times 10^3$ Pa/m [65].

A conservative (non-degrading, non-sorbing) tracer (1,6-naphthalene disulfonate according to [64]; 1,5-naphthalene disulfonate according to [62]) was injected. Injection continued over five hours [66], which is a short enough time that it may be considered instantaneous. The rate of fluid injection was 800 gpm (50 l/s), corresponding to a hydrodynamic admittance $A = 10$ l/s-bar = 10 l/s-MPa.

Tracer was first observed at the production well about 15 hours after injection, and its concentration rose to about $1/e$ of its maximum value about 50 hours after injection. Using this latter value to estimate the fluid velocity in a nominal crack, we find $v \approx 3 \times 10^{-3}$ m/sec (diffusion is expected to rapidly homogenize the tracer across the width of a crack). This value is much less than the characteristic v_0 defined in Section 4.4.1, and for the given pressure gradient, if this were a single crack, then $b = 0.0034\,\mathrm{cm} \ll b_0$. The corresponding Reynolds number $\mathrm{Re} \approx 0.3$.

The flow rate in such a crack $Q = 0.06$ l/s. This result is only 10^{-3} of the injected flow rate (50 l/s), which is consistent with $\mathcal{O}(1000)$ comparable cracks contributing to the flow. The fact that tracer is first detected after about 15 hours implies that there are some cracks in which v is about three times greater, and b about twice as large, but the fact that at this early time the tracer concentration is only about 10^{-3} of its peak value implies that very little mass flows through these larger cracks.

If there are $\mathcal{O}(1000)$ cracks in a resource of size $\mathcal{O}(0.5)$ km, the typical

distance between cracks is $\mathcal{O}(0.5)\,\mathrm{m} \ll \ell_T$ for $t_r \gg 1$ week. On any time scale relevant to extracting energy (but not necessarily in a brief experiment) if the cracks are identical and distributed uniformly the rock temperature will vary little in directions perpendicular to the fluid flow and (provided $b \ll b_0$, as inferred) the produced water temperature T_w would be very close to T_r.

4.5.3 Analyzing tracer breakthrough curves with a one-dimensional model

We next consider a more quantitative assessment of a breakthrough curve by trying to eliminate trial-and-error fitting, while offering a rapid, easy-to-use approach suitable for someone working in the field. We can expect that we do not know three important parameters in the field test: the mean speed v, the dispersion coefficient $\mathcal{D}$, and the fracture opening b; only the first two parameters enter directly the breakthrough analysis above. Of course, we are assuming that the one-dimensional analysis is applicable; such analyses are occasionally described in similar terms in the literature (e.g. [55, 56]).

We use the dimensionless form of the one-dimensional analysis described above, equations (4-11 to 4-12). Let us define the time τ_m of the peak normalized concentration C_m (see Figure 4-10), the time $\tau_{1/2} = \frac{1}{2}\tau_m$ corresponding to the concentration $C_{1/2}$, and the time $\tau_4 = 4\tau_m$ corresponding to the concentration C_4. Manipulation of equation (4-11) then leads to

$$\frac{3\left(4\tau_m^2 - 1\right)}{2\left(2 + 3\tau_m - \tau_m^2\right)} = \frac{\ln\left(2C_4/C_m\right)}{\ln\left(C_{1/2}/\left(C_m\sqrt{2}\right)\right)}. \tag{4-13}$$

The right-hand side is simply evaluated based on the 3 concentrations C_m, $C_{1/2}$ and C_4 and the units used for concentration do not matter as this formulation only involves ratios of concentrations. Then τ is evaluated by inspection of Figure 4-12. Alternative, a simple root-finding algorithm on a laptop (e.g. using Mathematica) readily yields a unique value of τ_m.

With τ_m in hand we determine v according to

$$v = \frac{\tau_m \ell}{t_m}, \tag{4-14}$$

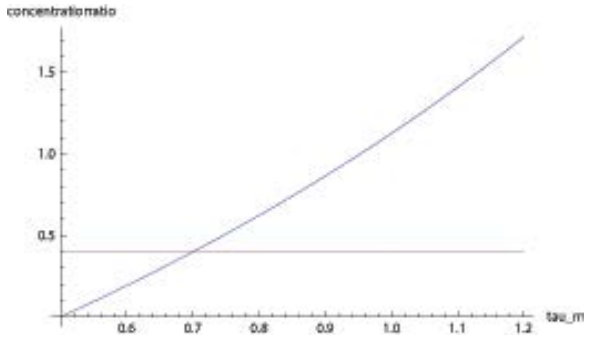

Figure 4-12: A plot of equation 4-13 where the right-hand side, is the vertical axis, here denoted "concentration ratio", is the input and then τ_m is read off the horizontal axis. The horizontal line is the value of the concentration ratio, here about 0.4, as determined from the data of Rose et al. [62] (Figure 4-11(a)).

where t_m is the time of the maximum concentration from the actual breakthrough curve. The Peclet number $\mathcal{P}_\ell$ for the tracer experiment is then determined rearranging equation (4-11) for two of the measured concentrations, e.g. C_m and C_4 according to

$$\mathcal{P}_\ell = -\frac{16\tau_m}{3\left(4\tau_m^2 - 1\right)} \ln\left(2C_4/C_m\right). \tag{4-15}$$

With $\mathcal{P}_\ell$ determined the longitudinal dispersivity for the data follows from

$$\mathcal{D} = \frac{v\ell}{\mathcal{P}_\ell}. \tag{4-16}$$

In this way, no trial-and-error fitting is required and, moreover, so long as the one-dimensional analysis is believed appropriate, the few steps above suffice to determine v and $\mathcal{D}$ from only 3 data points on a measured breakthrough curve.

Example: Using the Soda Lake data of Rose et al. [62], we find the right-hand side of equation (4-13) is ≈ 0.4 so that $\tau_m \approx 0.7$. Thus, we then determine $v \approx 9 \times 10^{-4}$ m/s, $\mathcal{P}_\ell \approx 3.1$ and $\mathcal{D} \approx 0.16$ m^2/s.

Moreover, with the values of v and $\mathcal{P}_\ell$ determined, we can show the quality of the fit to the data. In particular, we make time dimensionless and normalize the concentrations by the peak value (at t_m). The comparison is

shown in Figure 4-13(a) and captures the major features of the experimental curve.

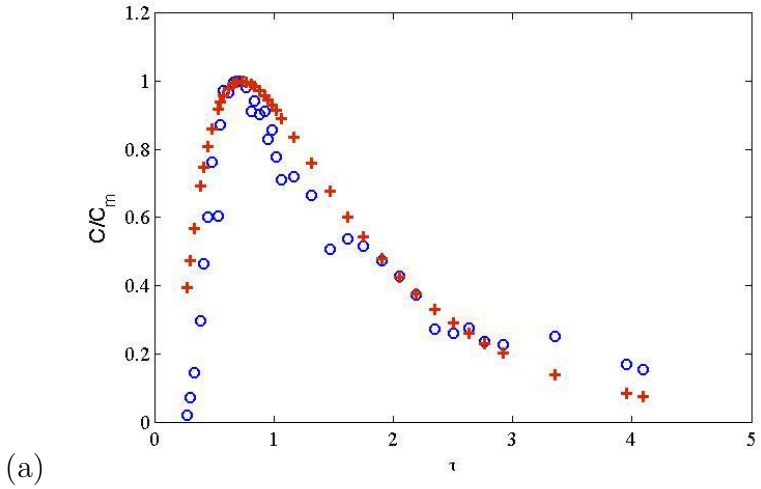

(a)

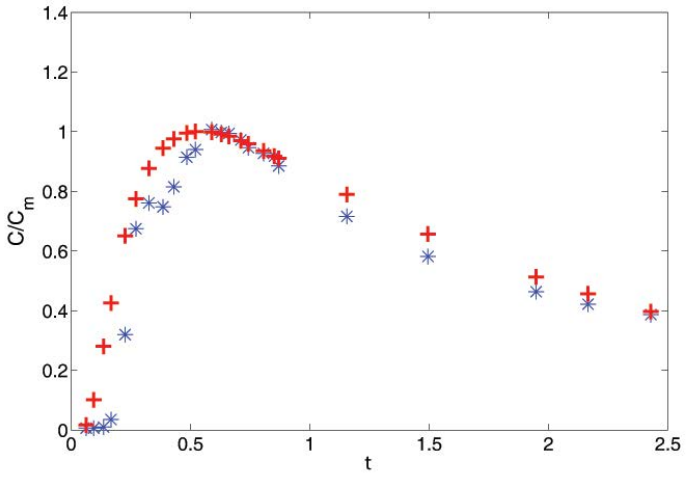

(b)

Figure 4-13: Comparison of the breakthrough data from Rose et al. (conserved, non-sorbing tracer), shown by the $*$ symbols, with the time-dependence, shown by the $+$ symbols, predicted by the one-dimensional analytical model, equation (4-11). (a) Soda Lake data [62]. (b) Steamboat data [63]. As described in the text, three data points are selected, v and $\mathcal{P}_\ell$ are calculated and the comparison is made.

We have performed a similar calculation for the non-sorbing tracer data available for the Steamboat geothermal site [63]. Here we estimate $\ell = 650$ m (based on Figures 2 and 3 in [63]) and find $\tau_m = 0.63$, which leads to $v = 6 \times 10^{-5}$ m/s and $\mathcal{D} = 0.027$ m^2/s. Again, as shown in Figure 4-13(b) we find that the one-dimensional analysis captures the major features of the experimental curve. Nevertheless, we are aware that this simplified analysis is not always so successful, as we found when analyzing data from the Soultz field [67] (though it may be possible to fit that data with a similar model involving two distinct values of τ_m, hence v and $\mathcal{D}$).

4.5.4 The dispersion produced by a network of cracks

There is a rich literature on dispersion in porous media, for which standard models consider packed beds of spheres, e.g. [60]. In addition, at the laboratory scale there are some studies of flow and dispersion in models characterized by "cracks" [68]; see Figure 4-14. Such models offer opportunities to better correlate spatial characteristics of a heterogeneous crack network with the resulting features, including the dispersivity, of tracer breakthrough curves. This kind of combination of laboratory-scale experiments and modeling, in conjunction with field-scale studies described above, offer one route for improved subsurface characterization.

4.6 Electromagnetic Imaging of Permeability

JASON proposes coupling tracer tests with electrically conducting fluids as one potential route to get more information about the spatial variations of the permeability in the neighborhood of injection and production wells. The idea is sketched in Figure 4-15. Since igneous rocks have electrical conductivities of about $10^{-6} - 10^{-3}$ S/m and sea water has electrical conductivities larger by at least 10^3, there are inexpensive options to inject a fluid, which can be identified relative to the rock, as the fluid migrates. In this way, injection tests, or injection-backflow tests, can yield valuable information on

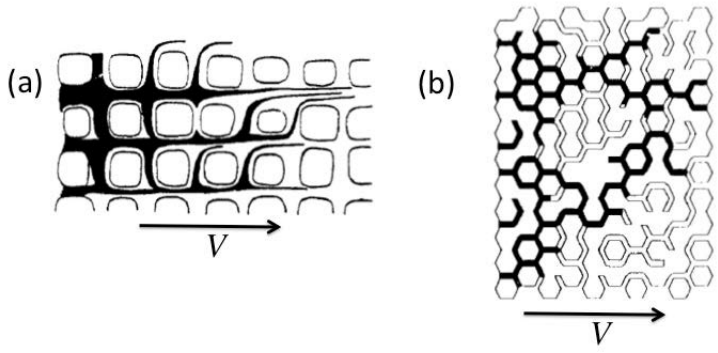

Figure 4-14: Schematics of two different two-dimensional network models for studying the dispersion of a tracer [68]. (a) A connected square lattice, where the channel width is random and the mean flow is parallel to one axis of the lattice. (b) Partly connected hexagonal lattice with uniform channel width where the network is above the percolation threshold; here the percolation parameter $p = 0.72$.

the permeability. For example, in the spirit of the one-dimensional tracer calculation shown above, it is straightforward to analyze a similar injection-backflow scenario to correspond with the kind of test sketched in Figure 4-15.

Magnetotelluric (MT) and other electromagnetic (EM) techniques are well established as means of characterizing the 3-D spatial distribution of fluids at depth, including in geothermal regions (e.g., [69]). Controlled-source MT is applicable to EGS-relevant depths [70], and short-range high-resolution methods such as GPR (Figure 4-1) can be applied to initial field experiments before one moves up to the spatial scales of production well-pairs [71]. Current state of the art applies joint inversion of multiple imaging methods, including seismic and gravity as well as EM (e.g., [72]–[75]). More controversially, imaging is improved if one can assume relationships between independently measured properties (e.g., seismic-wave velocity and electrical resistivity [75]–[77]), which may be reasonable for permeable zones of interest in geothermal applications.

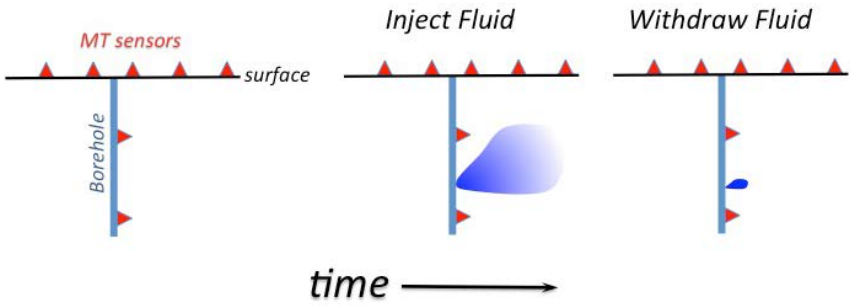

Figure 4-15: Schematic of an injection-backflow tracer test with an electrically conducting fluid, coupled with surface (and possibly borehole-emplaced) electromagnetic imaging to monitor spatial-temporal dynamics. Continuous temperature logging (e.g., by a fiber-optic probe) is also proven as an important tool for monitoring flow out of boreholes.

The specific approach we advocate is to monitor time-dependent changes in EM response through a combination of surface- and, to the degree possible, borehole-based measurements of electrical resistivity at depth (Figure 4-15). MT has been successfully applied to monitor EGS fluid injection, for example [78, 79], and time-dependent cross-well imaging is used for near-surface applications that may be relevant to initial (short-range) field experiments [80, 81].

4.7 Enhanced Subsurface Validation Made Possible by Micro Drilling

Micro drilling offers opportunities for enhanced subsurface characterization. Here we indicate possible ways that the use of micro drilling could be used to validate and improve models related to permeability of the reservoir, the fracture/flow network, and the interpretation of tracer (or other) tests.

All field-scale studies are based on spacings between injection and production wells, which typically are hundred of meters, if not actually several times more. It appears to JASON that using micro drilling to produce field tests with more closely spaced wells, e.g. tens of meters, can be used to test

various assumptions. For example, in all models (even ad hoc models) of flow and heat transfer in the subsurface the distance between the injection and production wells is a variable. Thus, micro drilling two wells at a spacing of tens of meters offers opportunities to more rapidly do various tests, e.g. tracer breakthrough experiments and heat transfer studies as a function of the applied pressure difference (or flow rate). In this way, the influence of the well spacing ℓ, the pressure drop Δp, the flow rate Q, the mean breakthrough time, the dispersion representative of a tracer experiment, etc. can all be tested and correlated (there would also be opportunity to use EM methods as described in the preceding section). Moreover, the variations of measured properties with time can also be performed in more controlled settings. In addition, when fracturing operations are performed, it is likely that the opportunities that micro drilling offers for getting improved spatial characterization of the flow field will be helpful in understanding better the creation of fracture networks in these subsurface environments.

Other kinds of tests can be envisioned. For example, with the kind of micro drilling approach above, perhaps combined with electromagnetic or seismic imaging, one can produce from multiple production wells, either in a line (so they are all on the same path) or on widely separated azimuths, simultaneously, i.e. pump whatever fluid is in the production well by reducing its pressure to zero. This approach might answer questions such as whether there is only one crack (or permeable zone) that might miss some of the wells, or if all rock out to some distance from the injection well is permeable. In addition, such a pumping test might answer a question such as "Does pumping from one well starve downstream wells, as it would in directed flow, or starve wells in all directions, as it would in diffusive flow?" Obviously, a new kind of field-site testing facility would raise other useful questions to address.

These types of operations can, in principle, offer ways to assess the spatial variation of the permeability in subsurface environments. For example, drilling one injection well and a series of production wells positioned at in-

creasing distances from the injection well allows for a systematic study by sequentially producing from only one well at a time. Then, flow experiments with first the closest production well opened, and then the next production well opened (with the first and all others closed), etc. should allow for improved understanding of spatial heterogeneities possible in subsurface environments.

References

[1] N. E. Todreas and M. S. Kazimi, *Nuclear Systems I: Thermal Hydraulic Fundamentals*, Taylor and Francis, New York, 720 pp (1989).

[2] Reimus, P., *et al. Thirty-Seventh Workshop on Geothermal Reservoir Engineering* (Stanford U., Stanford, Cal. 2012) SGP-TR-194.

[3] Rose, P., *et al. Thirty-Seventh Workshop on Geothermal Reservoir Engineering* (Stanford U., Stanford, Cal. 2012) SGP-TR-194.

[4] Reimus, P. email to J. Katz July 24, 2013.

[5] Rose, P. email to J. Katz July 25, 2013.

[6] Rose, P. E. and Adams, M. C. *Geothermal Resources Council TRANSACTIONS* **18**, 237–240 (1994).

[7] Fine, R. A. and Millero, F. J. *J. Chem. Phys.* **59**, 5529 (1973).

[8] Jung, R. *EGS — Goodbye or Back to the Future*, Chap. 5 pp. 95–121 `http://dx.doi.org/10.5772/56458` (2013).

[9] Grant, M. A. and Garg, S. K. *Thirty-Seventh Workshop on Geothermal Reservoir Engineering* (Stanford U., Stanford, Cal. 2012) SGP-TR-194.